

Numerical Simulation of Direct Contact Membrane Desalination in Conjugate Heat Transfer Configuration: Role of Membrane Conductivity

Isam Janajreh*, Dana Suwwan

Mechanical Engineering Program, Masdar Institute of Science and Technology, PO Box 54224, Abu Dhabi, UAE

Abstract

The Abstract- Direct Contact Membrane Distillation (DCMD) is modeled using conjugate heat transfer Navies-stokes flow model. A uniform salty and relatively hot feed and colder fresh permeate flow driven by peristaltic pump are considered in parallel configuration across the membrane. Depending on the membrane parameters (permeability, thickness, pour size and conductivity) the resulted temperature difference lead to pressure gradient responsible for the vaporizing fraction of the feed and transport to the permeate side through the hydrophobic membrane. Under different flow condition and membrane conductivity mass flux, heat flux, temperature polarization and thermal efficiency are evaluated. Results showed a good agreement with the published theoretical work on the mass flow this followed with sensitivity study to two parameters one is operational and the other is design to gain better understanding of the system performance and metrics including temperature polarization, convective and conductive heat flux, and associated latent heat of evaporation.

Keywords: *Direct Contact Membrane Distillation, Mass Transfer, Heat Transfer, Temperature Polarization*

1. Introduction

Direct contact membrane distillation (DCMD) is gaining more popularity because of the required low-grade energy compared to other technologies such as MSF or RO [1]. The advantages of the DCMD lies in its simplicity, utilization of a low-grade temperature difference and the potential of achieving near 100% rejection of dissolved solids [2]. In addition, membrane processes can be modular and flexible for scale up, keeping the advantage that separation is occurring under mild conditions [3]. Another benefit lies in the variable membrane properties, which can be adjusted. A review on the design of membrane distillation can be found elsewhere [4,5] which includes, in addition to the DCMD, air gap membrane distillation (AGMD), vacuum membrane distillation (VMD), and sweeping gas membrane distillation (SGMD) as illustrated in figure 1 below.

The DCMD includes phase-change at the feed side, transmembrane flux towards the permeate side, and condensation at the permeate side [4]. It is different from the classical multistage flash (MSF), multi-effect distillation (MED), vapor compression (VC), freezing, and humidification/dehumidification, solar stills electro-dialysis (ED), reverse osmosis (RO), and common membrane distillation (MD) [1]. Many of these common techniques are operated by the consumption of large amounts of fossil fuels to power dedicated desalination plant or indirectly through co-generation. DCMD is a well-known water production application providing separation and purification.

The anatomy of the DCMD consist of two-flows with different temperatures and species separated by a hydrophobic membrane, which is in direct contact to the flow. The feed flow is typically the flow with higher temperature than the permeate flow. The temperature difference between the two flows across the contacting membrane surface creates a difference in the potential vapor partial pressure. This difference drives the transport of vapor mass and energy transfer from the hotter feed side to the cooler permeate side.

This work aims at obtaining fundamental understanding of the DCMD setup and its pronounced parameters through high fidelity numerical flow simulation and sensitivity study. DCMD's pure water productivity has been presented in several macroscopic models. Several empirical and semi-empirical models were also proposed [3]. Lately, a model that includes the temperature polarization for a flat DCMD was proposed, this model was helpful in understanding the transmembrane flux mechanism. Hui Yu et al. conducted a numerical study considering the transmembrane heat and mass fluxes of the DCMD membrane in a hollow fiber tube [6]. They utilized similar conjugate heat transfer model and studied the influence of the mass flow and length of the membrane but with less emphasis on the combined width, length, velocity effect. Others utilized less accurate semi-empirical correlation, constant mass flux coefficient, single side of the flow, or stack of thermal resistances to arrive to the prediction of the driving process temperature distribution [2, 7-10]. Zhang et al. [7, 11] are amongst the pioneer who modeled the DCMD as conjugate heat considering the membrane and its surrounding fluid, yet without consideration of any phase change. The mean spatial

* Corresponding author. Tel.: +97128109130

Fax: +9876543210; E-mail: ijanajreh@masdar.ac.ae

© 2014 International Association for Sharing Knowledge and Sustainability

DOI: 10.5383/swes.06.02.009

temperature was also estimated by the work Fane et al. using the boundary layer analogy [12, 13]. However, due to strong coupling of the two fluid sides and the semi conductive membrane and its transmembrane flux these empirical models fall short to provide reliable and comprehensive flow information to the two-dimensional temperature distribution and thereby to the spatial heat transfer coefficients [4, 14]. These findings considered both parallel and counter flow arrangement. Results of CFD simulations and experimental work were compared in terms of mass fluxes and temperature distributions. They found that, temperature polarization decreases upstream and then increase downstream. The local heat fluxes increased and then decreased with the flow direction. Nusselt number was also reported to be highest at the entrance due to thin thermal boundary layer and prior to the developing flow. Most importantly, the thermal efficiency, which defined as the heat carried by the transmembrane flux to the total heat, was studied and it was found that higher velocities does in fact enhance the transmembrane mass flux, however decreases the efficiency due to heat loss on the permeate side due conduction.

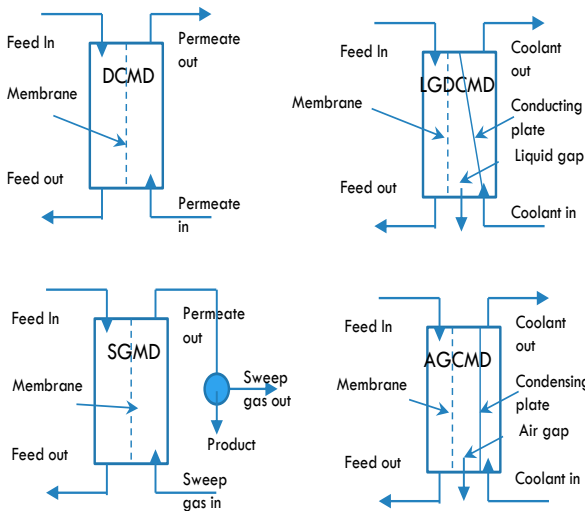


Fig. 1. Different DCMD configuration

High fidelity and rather complicated fluid dynamics modeling combined with Ergun model for pressure drop, Knudson-diffusion for transmembrane flux, was introduced by Carfi et al. [15] for the modeling of the DCMD. The brought complexity of this model, however, hindered its practicality. Therefore, only limited literature on the high fidelity CFD modeling of the DCMD presents today. This work intend to enrich this literature gap by considering a comprehensive arrangement of the flow in two dimensional laminar Navies-stokes flow coupled with the energy conservation for the membrane in a conjugate heat transfer. This model is equally applied to parallel (or counter flow) channels as well as axisymmetric of two concentric cylindrical flow separated by the membrane. Such model can be used as conceptual design tool for innovative design and development in the new emerging field of DCMD.

2. Theoretical Model

Schematic of the studied DCMD in horizontal configuration is illustrated in figure 2. Overall, an aqueous hot feed (Hot channel) enters the top side (outer cylinder in axisymmetric) of

the membrane, while the permeate enters the bottom cold side of the membrane (inner cylinder axisymmetric). Evaporation of the feed first occurs at the top/outer membrane surface in the form of pure water, and vapor is then transported within the membrane towards the bottom surface and finally this vapor condensates on that surface as pure permeate [17]. The performance of the DCMD depends on the temperature of the feed/permeate flows, temperature and pressures and physical membrane characteristics, permeability, conductivity, pour size and distribution, and thickness.

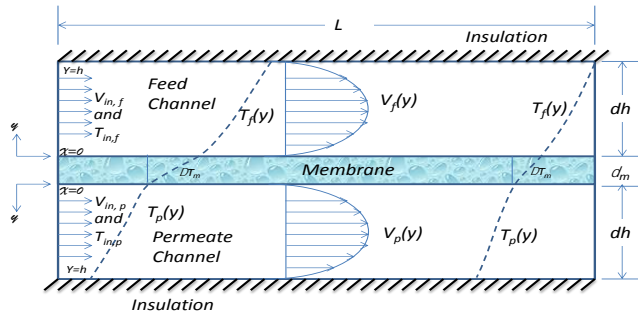


Fig.2 Schematic diagram of parallel-flow DCMD

For the modeling purposes, we have assumed two-dimensional (2D) model following the Cartesian coordinates along the x and perpendicular to y directions. The incoming velocity profiles are considered uniform and parallel flow at fixed velocity and temperature values.

2.1 Governing Equations

For the consideration steady state heated flow process, the mass and x and y Navies-stokes (momentum) conservation are given in equations 1, 2a, and 2b, respectively.

$$\frac{\partial(\rho u)}{\partial x} + \frac{\partial(\rho v)}{\partial y} = 0 \tag{1}$$

$$u \frac{\partial(\rho u)}{\partial x} + v \frac{\partial(\rho u)}{\partial y} = -\frac{\partial P}{\partial x} + \mu \left(\frac{\partial^2 u}{\partial x^2} + \frac{\partial^2 u}{\partial y^2} \right) \tag{2a}$$

$$u \frac{\partial(\rho v)}{\partial x} + v \frac{\partial(\rho v)}{\partial y} = -\frac{\partial P}{\partial y} + \mu \left(\frac{\partial^2 v}{\partial x^2} + \frac{\partial^2 v}{\partial y^2} \right) + \rho g_y \tag{2b}$$

Where $\rho \left(\frac{kg}{m^3} \right)$, $u \left(\frac{m}{s} \right)$, $v \left(\frac{m}{s} \right)$, $P(pa)$, and $\mu (pa \cdot s)$ are the density, velocity in x, velocity in y, pressure and dynamic viscosity, respectively. The scalar energy equation is also given by:

$$u \frac{\partial(\rho CpT)}{\partial x} + v \frac{\partial(\rho CpT)}{\partial y} = k \left(\frac{\partial^2 T}{\partial x^2} + \frac{\partial^2 T}{\partial y^2} \right) + S_h \tag{3}$$

Where $Cp \left(\frac{W}{kg \cdot K} \right)$, $T (k)$, and $k \left(\frac{W}{m \cdot K} \right)$ are the specific heat, temperature, u velocity in x, v velocity in y, and k is the thermal conductivity, respectively.

The S_h signifies the sink/source heat that is attributed to the latent heat of evaporation at both the feed and permeate membrane surface, respectively. It can be defined following the work of Yu et al as:

$$S_h = \begin{cases} \frac{q_{md}}{\delta_y} \cdot \frac{y_{mo}}{y_{mi}} \text{ for } y = y_{mi} \\ -\frac{q_{md}}{\delta_y} \text{ for } y = y_{mi} \\ 0 \text{ otherwise} \end{cases} \quad (4)$$

Where the q_{md} is the membrane's feed side latent heat flux, y is the vertical distance and the subscripts mo and mi signifies the locations of the top and bottom membrane surfaces, respectively. The S_h also holds the heat boundary conditions attributed to the flow and implicitly applied to the membrane surface.

2.1.1 Mass Flux

In the DCMD process, evaluating the transport of mass constitutes the process productivity. Due to the temperature gradient, a driving pressure force is created which is responsible for the mass transfer across the membrane [3]. The general form of the mass flux is illustrated by Chen and Greenlee [3, 1], which is written as:

$$J'' = c_m (P_{mf}^{sat} - P_{mp}^{sat}) \quad (5)$$

Where c_m , P_{mf}^{sat} , and P_{mp}^{sat} are the intrinsic mass membrane coefficient, saturated pressure of water on the feed and permeate membrane's surface, respectively. The beauty of the above equation is for a given pressure-temperature relation the mass flux temperature dependency can be inferred such that:

$$J'' = c_m \frac{d}{dT} (P_{mf}^{sat} - P_{mp}^{sat}) * (T_{mf} - T_{mp}) \quad (6)$$

The pressure temperature relation is tabulated in steam tables according to Antoine equation [12] which follows a monotonic form within the operational desalination temperature range. This equation is written as:

$$P_{pure}^{sat} = \exp \left(23.238 - \frac{3841}{T_m - 45} \right), i \in \{f, p\} \quad (7)$$

This equation is adjusted for none pure saline or waste water as shown in our previous work [14].

$$P_i^{sat}(x, T) = x_w a_w P_{i(pure)}^{sat}, i \in \{f, p\} \quad (8)$$

Where x_w , a_w are the mole fraction of the water in saline solution and the water activity in NaCl solutions, respectively. The temperature is expressed in Kelvin degree (K), and the pressures are given in Pascals (Pa). The water activity in NaCl solutions is estimated using correlation of Khayet [4] and Lawson [2] as:

$$a_w = 1 - 0.5x_{NaCl} - 10x_{NaCl}^2 \quad (9)$$

Where x_{NaCl} is the mole fraction of NaCl in the brine solution. Therefore, an increase in temperature will definitely lead to an increase in the transmembrane mass flux. This can be achieved either by operating at higher feed temperature condition or by targeting a higher temperature distribution along the membrane.

The mass coefficient is obtained from the simulation following either Knudson-diffusion, molecular diffusion, Poiseuille flow or Monte Carlo simulation as reported by Ding et al [18], Bui et al [19] and Imdakum and Mussarra [20].

This work uses a suitable combination between Knudson and Poiseuille models as was presented by Chen et al. [4] and is described as:

$$c_m = c_k + c_p = 1.064 \alpha(T) \frac{\epsilon r}{\tau \delta_m} \sqrt{\frac{M_w}{R T_{mt}}} + 0.125 \beta(T) \frac{\epsilon r^2}{\tau \delta_m} \quad (10)$$

Where $\alpha(T)$, and $\beta(T)$ are Knudsen diffusion model and Poiseuille flow model contributions, respectively. M_w is the molar mass of the water in (kg/mol), T_{mt} is the mean membrane temperature (C), R is the gas constant, P_m is the mean pressure, δ_m is the thickness of the membrane, η_v is the gas viscosity, r is the pores radius, ϵ is the porosity of the membrane, τ is the tortuosity factor, which can be estimated for hydrophobic membrane by Iversen et al. [21] such as:

$$\tau = \frac{1}{\epsilon} \quad (11)$$

The transmembrane heat flux is described by the latent heat flux and conduction through the membrane. The former is written as:

$$q_m = j'' \cdot \Delta H_m \quad (12)$$

Where ΔH_m is the latent heat of the transmembrane fluid that permeated. The conduction is described by the Nusselt number such that:

$$Nu = \frac{h \cdot d}{k} \text{ or } \frac{q \cdot d}{k(T_b - T_m)} \quad (13)$$

Where h , d , and k are the heat transfer coefficient, characteristic length and thermal conductivity. The q and is the heat flux and T is the local temperature where the subscripts b and m signify the bulk and the membrane, respectively.

2.1.2 Heat Flux

The heat transfer in DCMD process can be described following three steps: The heat transfer through the feed boundary layer, heat transfer through membrane, and heat transfer through the permeate boundary layer [17]. The total heat flux for the membrane is either due to the convection through the feed membrane surface, or the convection through the permeate membrane surface or a combination between the conduction (Q_m) and latent heat of evaporation through the membrane. The conduction across the membrane material is in part due to the bulk membrane material conduction (Q_c) and the other is due to the vapor-filled pores (Q_v). The total membrane heat flux can be described as:

$$Q_m = Q_c + Q_v \quad (14)$$

The transmembrane heat flux is written as:

$$q_m = j'' \cdot \Delta H_m \quad (15)$$

Where ΔH_m is the latent heat of the transmembrane flux of the fluid which according to Termpiyakul et al. [16], this enthalpy can be fitted from the enthalpy data of saturated water vapor and liquid according to the following equation:

$$H_{m,i} = 1.7535 T_{m,i} + 2024.3 \quad i \in \{f, p\} \quad (16)$$

Hence the The conduction is expressed as:

$$Q_{m,i} = \frac{k_m}{\delta_m} (T_{m,f} - T_{m,p}) \quad (17)$$

with $K_m = (1 - \varepsilon)K_b + \varepsilon K_v$

Where k_m is the membrane conduction coefficients, T is the temperature and f and p signify the feed and permeate respectively. The K_m is the total membrane conductivity which volume weighted average of the bulk conductivity K_b and is the vapor conductivity K_v which can be estimated from the work of Chen and Ho [3]. The convective heat transfer coefficient can be described by the Nusselt number such that:

$$Nu = \frac{h.d}{k} \text{ or } \frac{q.d}{k(T_b - T_m)} \quad (18)$$

Where h , d , and k are the convective heat transfer coefficient, characteristic length and thermal conductivity. The q above is the heat flux and T is the local temperature where the subscripts b and m signify the bulk and the membrane, respectively.

2.1.3 DCMD Metrics

DCMD thermal efficiency (η): This metric is governed by the fraction of the heat used as latent heat of evaporation instead of the lost conduction fraction. This efficiency can be written as:

$$\eta = j'' \cdot \Delta H_m / q_f \quad (19)$$

Where $q_f = j'' \cdot \Delta H_m + K_m (T_{mf} - T_{mp}) / \delta_m$ (20)

Therefore, low membrane conductivity is desirable to increase the thermal efficiency. Dividing by the latent heat enthalpy (ΔH_m) defines the “equivalence” conductive mass flux (j''_{keq}) and hence the efficiency can be rewritten as:

$$\eta = j'' / (j'' + j''_{keq}) \quad (21)$$

Eq. 21 states another definition to the membrane desalination/filtration efficiency; it is the ratio of the transmembrane flux to that of the total theoretical mass flux when ignoring any lower grade heat losses such as frictional or radiative heat.

Evaporation Efficiency: It is defined as the ratio of heat involved in evaporation in comparison with the heat difference along the channel for either the distillate or feed flow [22].

$$\eta = \frac{j'' \Delta H_v A_t}{\dot{V}_{distillate} c_p \Delta T_p} = \frac{j'' \Delta H_v A_t}{\dot{V}_{feed} c_p \Delta T_f} \quad (22)$$

Temperature polarization (θ): It measures the ratio of boundary layer resistance over the total heat transfer resistance, and is written as:

$$\theta = \frac{T_{m,f} - T_{m,p}}{T_{b,f} - T_{b,p}} \quad (23)$$

Where the subscripts m, b, f, p signify the membrane, bulk, feed flow and permeate flow, respectively. For small θ (≤ 0.2), the DCMD is considered heat transfer limited meaning the module design is poor. For larger θ value (≥ 0.6),

the DCMD enters the mass transfer limitation that is hindered because of the low membrane permeability [16]. The presented mathematical and CFD models are applied to determine the mass flux, heat flux, temperature polarization, and membrane coefficient for the parallel flow.

2.1.4 Flow Properties and Boundary Conditions

The geometry of the problem admits both 2D and axisymmetric configurations, while only the 2D is adopted in this work. The baseline geometry consisted of 21cm length by 0.1cm width of each channel. The membrane is sandwiched in between the two channels with a 0.130mm thickness. The flow is considered parallel flow entering at nominal Reynolds number of 500 and inlet feed temperature of 40°C and 25°C for the permeate. A quadrilateral mesh type is used for the whole geometry, feed channel, permeate channel and the membrane. A boundary layer mesh is used at the membrane surface targeting $y+$ value of one unit. It progressively and smoothly expanded towards the center channel. The mesh size is 2,100x64 and 2,100x8 for the membrane. Material properties of each of the membrane, salt feed water and permeate fresh water are summarized in table 1. Initially the property of the membrane is evaluated using a void-solid weighted average according to the following equation:

$$\phi_m = (1 - \varepsilon)\phi_o + \varepsilon\phi_v \quad (24)$$

Where ϕ is the equivalent permeable membrane property and the subscripts o and v signify the core membrane material (typically is polyvinidene fluoride or polyvinyl alcohol) and the vapor which occupies the membrane pores.

Table 1: Properties of the of membrane and flow materials

Material	Density (kg/m ³)	Specific heat (J/kg.k)	Conductivity (w/m.k)	Viscosity (Pas)
PVDF [23]	1175	1325	0.2622	-
Vapor	0.554	2014	0.0261	-
Membrane	302.2	1896.9	0.0662	-
Saline sea water* [24]	1013.2	4064.8	0.642	5.86E-4
Pure water** [25]	995.2	4182.1	0.613	8.38E-4

*At 3.5% salinity and 323 K; **At 303K

3. Results and Discussions

Temperature field: Result of the temperature profile is depicted in figure 3, it is favorably compared to Chen et al work. It is noticed a considerable influence of the flow velocity on the temperature distribution at the membrane surface and this difference grows larger as the velocity is increased/doubled and it became more pronounced when the velocity is quadrupled as depicted in figure 3. The difference in temperature is maintained until the flow exit. It is however not easy to state the optimal velocity values as both the one sided bulk and membrane surface temperatures are decrease asymptotically. The shorter residence time for the flow to cool down at the feed side, or to heat up at the permeate side however slows the trend at higher velocities. These results are in agreement with those obtained by Chen et al. [17] as shown in figure 3b. It is worth mentioning that the mean membrane temperature is almost constant and nearly identical for the parallel flow in the DCMD model corresponding to the three velocity values.

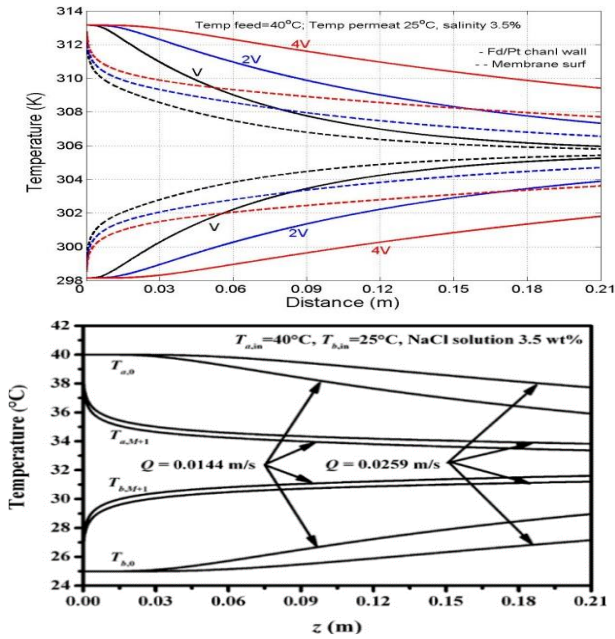


Fig. 3. Temperature profiles correspond to different mass flow (inlet velocity) for parallel flow in which the feed is entering at 40°C and the permeate is at 25°C.

Figure 4 depicts the temperature distribution for the top feed wall, feed membrane surface, permeate membrane surface and bottom permeate wall respectively for different values of membrane conductivity k_1, k_0, k_2 & k_3 (0.05, 0.178, 0.5 & 1). As a rule of thumb a lower conductivity that is (k_1) must allow the temperatures to take longer to reach steady value along the membrane. In addition, this means the temperature difference across the channel must be the highest for conductivity k_1 , which indeed is reflected in the distribution above. As the conductivity increases from k_1 - k_3 , the temperature trends get narrower allowing a small difference.

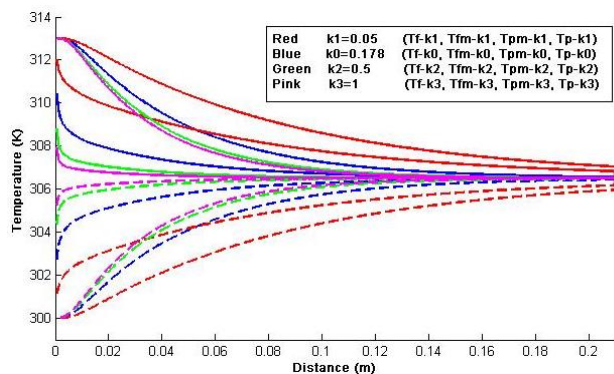


Fig. 4. Temperature distributions for feed and permeate wall and membrane surface for different membrane conductivities. Because of this temperature difference, lower conductivity creates a higher temperature difference, leading to a linear impact on the pressure difference, and thus enhancing the mass permeate flux through the membrane. Therefore, we do expect a higher mass flux once the membrane conductivity is lowered.

Plot of Nusselt number is depicted in figure 5. It is characterized with relatively low values as expected. A slightly higher value is favoring the feed side due to the higher temperature and with a sharp to asymptotic decrease at the entry downstream along the channel length.

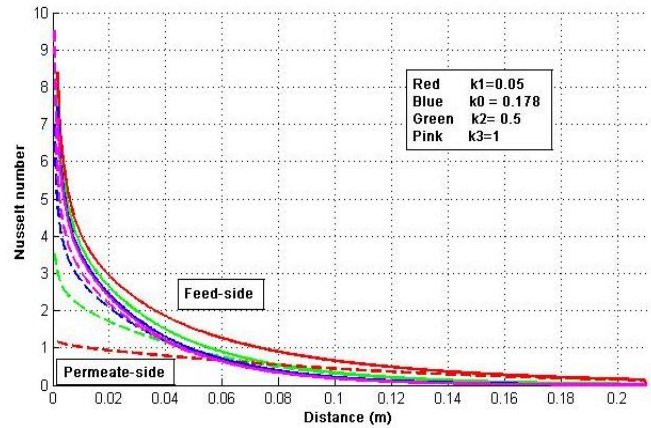


Fig. 5. Nusselt numbers for both the feed-side and permeate side (dotted lines) for k_1, k_0, k_2 and k_3

The accumulative mas flux is also calculated and is shown in table. It shows higher value for the lower conductivity k_1 (0.05) conductivity in comparison to k_3 (1). As expected from the temperature distribution, mass flux is enhanced by keeping the conductivity of the membrane as low as possible. The table below represents the accumulative mass flux for these conductivities.

Table 2: Accumulative mass flux for the different membrane conductivity value

Conductivity	Mass Flux (kg/m ² .hr)
$k_1 = 0.01$	3.218
$k_0 = 0.178$	1.571
$k_2 = 0.5$	1.102
$k_3 = 1$	0.971

Heat flux across the membrane is depicted in figure 6 and 7. It incorporates the heat loss through conduction and the latent heat of vaporization that takes place. The analogy here is, conductance heat loss is dominant in general since the thickness of the membrane is very low, however, it decreases by lowering the conductivity, the latent heat of vaporization increases since as it is function of mass flux. Therefore, as an outcome the heat flux associated with k_1 is higher than k_3 .

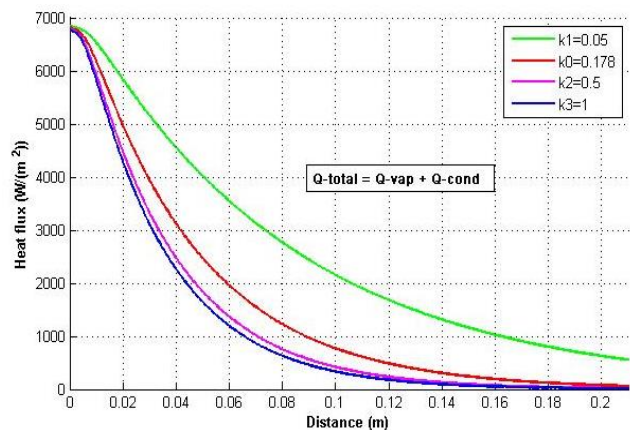


Fig. 6. Total Heat flux for different conductivity

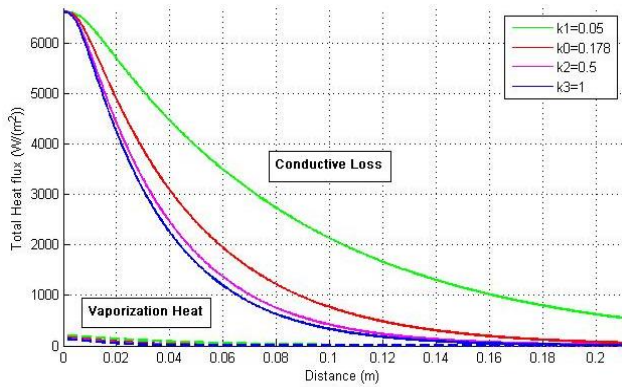


Fig. 7. Conductive and Vaporization heat for the different conductivity

Thermal and evaporation efficiencies of the DCMD system are depicted in figures 8 and 9. The efficiency is highest for k_1 (0.05) and that is indeed due to the fact that latent evaporation to total heat flux is higher. One can however observe the low overall efficiency which is of a few percentiles, but having the technology operable at low temperature difference overweight such low efficiency.

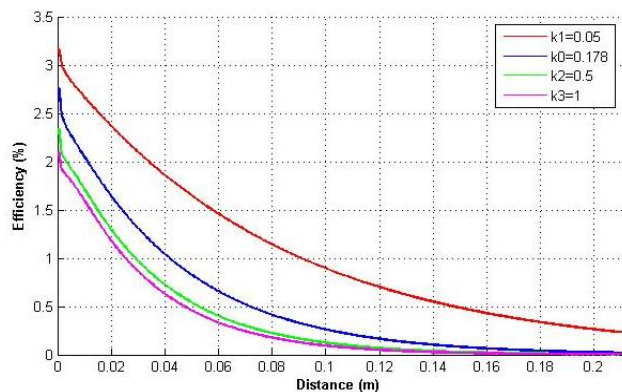


Fig. 8. Thermal efficiency of DCMD for k_1 , k_0 , k_2 and k_3

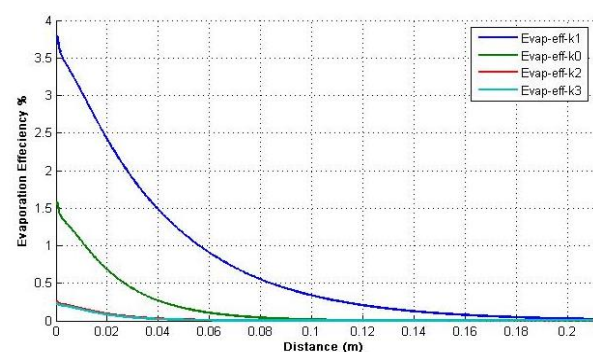


Fig. 9. Evaporation efficiency for k_1 , k_0 , k_2 and k_3 .

4. Conclusion

The conjugate heat computational fluid dynamics model was developed to assess the performance of DCMD corresponding to different velocity and membrane conductivity. The model evaluates and returns the bulk temperature and membrane temperature at the two sides of the two parallel flow representing the hot feed and cold permeate. The temperature gradient across the membrane create a difference in the

saturation pressure across the membrane fluid, which drives mass and energy transfer through the membrane from the feed to the permeate side. The model is utilized to investigate local and accumulative flow parameters. Including the mass flux, the heat flux and the DCMD metrics. The increase in the inlet flow resulted in a higher values of mass flux this is due to the higher convective heat flux as illustrated by the higher values of Nusselt number. Temperature polarization was investigated. Beyond the entry region, neither heat nor mass transfer limitation occurs as the TP values remain within the recommended range, i.e. {0.2, 0.6}. In view of these results, the efficiency of the process is evaluated and found to be low for once through. Therefore, detailed sensitivity analysis is suggested to find the optimal yield and process metrics. The model also studied the effect of membrane conductivity over the temperature distribution, Nusselt number, mass and heat flux and efficiency. The findings suggest a lower membrane conductivity allows a higher temperature difference across the channel which in fact creates a higher-pressure difference leading to an increase in the mass flux. The loss in conductance decreases alongside with an increase in latent heat of evaporation therefore resulting in higher efficiency.

Acknowledgments

The authors are grateful for the financial support from MASDAR Institute of Science & Technology and for all their team members of the Waste to Energy Laboratory for their support throughout this research.

References

- [1] L.F. Greenlee, D.F. Lawler, B.D. Freeman, B. Marrot, P. Moulin, "Reverse osmosis desalination: water sources, technology, and today's challenges", *Water Res.* 43 pp. 2317–2348, 2009.
- [2] K.W. Lawson, D.R. Lloyd, Membrane distillation. II. Direct contact MD, *Journal of Membr. Science* 120 pp. 123–133 1996.
- [3] T. Chen, C. Ho. "Immediate assisted solar direct contact membrane distillation in saline water desalination", *Journal of Membrane Science* 358, pp. 122-130, 2010
- [4] M. Khayet, T. Matsuura "Membrane Distillation, Principles and Applications" ELSEVEIER, 2011
- [5] M.C. de Andrés, J. Doria, M. Khayet, L. Peña, J.I. Mengual, "Coupling of a membrane distillation module to a multieffect distiller for pure water production" *Desalination* 115 pp. 71–81, 1998.
- [6] Hui Yu, Xing Yang, Rong Wang, Anthony G.Fane, "Numerical simulation of heat and mass transfer in direct membrane distillation in a hollow fiber module with laminar flow" *Journal of Membrane science*, 2011.
- [7] L.-Z. Zhang, C.-H. Liang, L.-X. Pei, Conjugate heat and mass transfer in membrane-formed channels in all entry regions, *Int. J. Heat Mass Transfer* 53 (5–6) (2010) 815–824.

- [8] M. Gryta, M. Tomaszewska, Heat transport in the membrane distillation process, *J. Membr. Sci.* 144 (1–2) (1998) 211–222
- [9] S. Aravinth, Prediction of heat and mass transfer for fully developed turbulent fluid flow through tubes, *Int. J. Heat Mass Transfer* 43 (8) (2000) 1399–1408.
- [10] M. Qtaishat, T. Matsuura, B. Kruczek, M. Khayet, Heat and mass transfer analysis in direct contact membrane distillation, *Desalination* 219 (1–3) (2008) 272–292
- [11] L.-Z. Zhang, Heat and mass transfer in a quasi-counter flow membrane-based total heat exchanger, *Int. J. Heat Mass Transfer* 53 (23–24) (2010) 5478–5486.
- [12] J. Phattaranawik, R. Jiraratananon, A.G Fane, “Heat transport and membrane distillation coefficients in direct contact membrane distillation” *Journal of Membrane Science* 212, pp. 177-193, 2003.
- [13] R.W. Schofield, A.G. Fane, C.J.D. Fell, “Heat and mass transfer in membrane distillation”, *J. Membr. Sci.* 33 pp.299–313.1987
- [14] I. Janajreh, D. Suwwan, H. Faith, ‘Numerical Simulation of low energy direct contact membrane desalination’, *International Journal of Thermal & Environmental Engineering*, 8, 133-138, 2014
- [15] K. Charfi, M. Khayet, M.J. Safi, Numerical simulation and experimental studies on heat and mass transfer using sweeping gas membrane distillation, *Desalination*, 259 (1–3), 84–96.
- [16] P. Termpiyakul, R. Jiraratananon, S. Srisurichan, “Heat and mass transfer characteristics of a direct contact membrane distillation process for desalination”, *Desalination* 177, pp. 133-141, 2009.
- [17] T. Chen, C. Ho, H.Yeh “Theoretical modeling and experimental analysis of direct contact membrane distillation”, *Journal of Membrane Science* 330, pp. 297-287, 2009.
- [18] Ding, Zhongwei; Liu, Liying; El-Bourawi, Mohamed S; Ma, Runyu, Analysis of a solar-powered membrane distillation system, *Desalination*, ISSN 0011-9164, 2005, Volume 172, Issue 1, pp. 27 – 40.
- [19] V.A. Bui, L.T.T. Vu, M.H. Nguyen, Modelling the simultaneous heat and mass transfer of direct contact membrane distillation in hollow fibre modules, *Membrane. Sci.* 353 (1–2) (2010) 85–93.
- [20] A.O. Imdakm, T. Matsuura, Simulation of heat and mass transfer in direct contact membrane distillation (MD): the effect of membrane physical properties, *J. Membr. Sci.* 262 (1–2) (2005) 117–128.
- [21] S.B. Iversen, V.K. Bhatia, K. Dam-Jphasen, G. Jonsson, “Characterization of microporous membranes for use in membrane contactors”, *Journal of Membrane Science*. 130, pp. 205-217, 1997.
- [22] M. Gryta, M. Tomaszewska, A.W. Morawski, Membrane distillation with laminar flow, *Sep. Purif. Technol.* 11 (2) (1997) 93–101.
- [23] Dhananjay Singh, Kamalesh K. Sirkar ‘Desalination of brine and produced water by direct contact membrane distillation at high temperatures and pressures’2011